PNAS

Supporting Information for

Definition of a saxitoxin (STX) binding code enables discovery and characterization of the anuran saxiphilin family

Zhou Chen[a†], Sandra Zakrzewska[a†], Holly S. Hajare[b], Aurora Alvarez-Buylla[c], Fayal Abderemane-Ali[a], Maximiliana Bogan[c], Dave Ramirez[c], Lauren A. O'Connell[c], J. Du Bois[b], and Daniel L. Minor, Jr.[a, d, e, f, g, h *]

[a]Cardiovascular Research Institute
[d]Departments of Biochemistry and Biophysics, and Cellular and Molecular Pharmacology
[e]California Institute for Quantitative Biomedical Research
[f]Kavli Institute for Fundamental Neuroscience
University of California, San Francisco, California 93858-2330 USA

[g]Molecular Biophysics and Integrated Bio-imaging Division
Lawrence Berkeley National Laboratory, Berkeley, CA 94720 USA

[b]Department of Chemistry
Stanford University, Stanford, CA 94305

[c]Department of Biology
Stanford University, Stanford, CA 94305

[†]Equal contributions

Correspondence to: Daniel L. Minor, Jr.

Email: daniel.minor@ucsf.edu

This PDF file includes:

Supplementary Materials and Methods
Figures S1 to S12
Tables S1 to S2
Legends for Movies S1 to S4
SI References

Other supporting materials for this manuscript include the following:

Movies S1 to S4

Supplementary Materials and Methods

Expression and purification of Sxphs and mutants

R. catesbeiana Sxph (*Rc*Sxph) and mutants were expressed using a previously described *Rc*Sxph baculovirus expression system in which *Rc*Sxph carries in series, a C-terminal 3C protease cleavage site, green fluorescent protein (GFP), and a His_{10} tag (*1*). The gene encoding *Nanorana parkeri* Sxph (*Np*Sxph) including its N-terminal secretory sequence (GenBank: XM_018555331.1) was synthesized and subcloned into a pFastBac1 vector using NotI and XhoI restriction enzymes by GenScript and bears the same C-terminal tags as *Rc*Sxph. *Rc*Sxph and *Np*Sxph mutants were generated using the QuikChange site-directed mutagenesis kit (Stratagene). All constructs were sequenced completely. *Rc*Sxph, *Rc*Sxph mutants, *Np*Sxph, *Np*Sxph I559Y, *Ma*Sxph, *Os*Sxph, and *Ri*Sxph were expressed in *Spodoptera frugiperda* (Sf9) cells using a baculovirus expression system as described previously for *Rc*Sxph (*1*) and purified using a final size exclusion chromatography (SEC) run in 150 mM NaCl, 10 mM HEPES, pH 7.4. Protein concentrations were determined by measuring UV absorbance at 280 nm using the following extinction coefficients calculated using the ExPASY server (https://web.expasy.org/protparam/): *Rc*Sxph Y558 mutants, 94,875 M^{-1} cm^{-1}; *Rc*Sxph F784C 96,490 M^{-1} cm^{-1}; *Rc*Sxph F784Y 97,855 M^{-1} cm^{-1}, *Rc*Sxph and all other *Rc*Sxph mutants 96,365 M^{-1} cm^{-1}; *Np*Sxph 108,980 M^{-1} cm^{-1}; *Np*Sxph I559Y 110,470 M^{-1} cm^{-1}; *Ma*Sxph 93,175 M^{-1} cm^{-1}; *Os*Sxph 100,625 M^{-1} cm^{-1}; and *Ri*Sxph 103 605 M^{-1} cm^{-1}.

Thermofluor (TF) assay of toxin binding

Thermofluor assays for STX and TTX binding were developed as outlined (*2*). TTX was purchased from Abcam (Catalog # ab120054). 20 µL samples containing 1.1 µM *Rc*Sxph, *Np*Sxph, *Ma*Sxph, *Os*Sxph, *Ri*Sxph, or mutants thereof, 5x SYPRO Orange dye (Sigma-Aldrich, S5692, stock concentration 5000x), 0-20 µM STX or TTX, 150 mM NaCl, 10 mM HEPES, pH 7.4 were set up in 96-well PCR plates (Bio-Rad), sealed with a microseal B adhesive sealer (Bio-Rad) and centrifuged (1 min, 230xg) prior to thermal denaturation. The real-time measurement of fluorescence using the HEX channel (excitation 515-535 nm, emission 560-580 nm) was performed in CFX Connect Thermal Cycler (Bio-Rad). Samples were heated from 25°C to 95°C at 0.2°C min^{-1}. Melting temperature (Tm) was calculated by fitting the denaturation curves using a Boltzmann sigmoidal function and GraphPad Prism: $F=F_{min}+(F_{max}-F_{min})/(1+\exp((Tm-T)/C))$, where F is the fluorescence intensity at temperature T, F_{min} and F_{max} are the fluorescence intensities before and after

the denaturation transition, respectively, Tm is the midpoint temperature of the thermal unfolding transition, and C is the slope at Tm (*2*). $\Delta Tm=Tm_{Sxph+20\mu M\ toxin}-Tm_{Sxph}$.

Fluorescence polarization assay

Fluorescence polarization assays were performed as described (*3*). 100 µL samples containing 1 nM fluorescein labeled STX (F-STX), 150 mM NaCl, 10 mM HEPES, pH 7.4, and Sxph variants at the following concentration ranges (*Rc*Sxph and *Rc*Sxph T563A, I782A, F784Y, D785N, Q787A, Q787E, K789A, and Y795A, 0-75 nM; *Rc*Sxph Y558A and I782A/Y558A, 0-24 nM; *Rc*Sxph Y558I, 0-37.5 nM; *Rc*Sxph Y558F, 0-100 nM; *Rc*Sxph I782F 0-150 nM; *Rc*Sxph F561A, 0-300 nM; *Rc*Sxph F784L, 0-500 nM; *Rc*Sxph E540D, P727A, and D785A, 0-600 nM; *Rc*Sxph F784A, 0-4.8 µM; *Rc*Sxph E540A and F784C, 0-10 µM; *Rc*Sxph D794A and D794E, 0-12.5 µM; *Rc*Sxph F784S, 0-17 µM; *Rc*Sxph D794N, 0-20 µM; *Rc*Sxph E540Q, 0-25 µM; *Np*Sxph; *Np*Sxph I559Y, 0-75 nM; *Ma*Sxph, 0-75 nM; *Os*Sxph, 0-75 nM; and *Ri*Sxph, 0-75 nM) were prepared in 96-well black flat-bottomed polystyrene microplates (Greiner Bio-One) and sealed with an aluminum foil sealing film (AlumaSeal II), and incubated at room temperature for 0.5 h before measurement. Measurements were performed at 25°C on a Synergy H1 microplate reader (BioTek) using the polarization filter setting (excitation 485 nm, emission 528 nm). Binding curves for representative high affinity (*Rc*Sxph, *Np*Sxph, and *Rc*Sxph-Y558I) and low affinity (*Rc*Sxph-E540D) proteins were compared at 0.5 h, 1.5 h, 4.5 h, and 24 h, post mixing and indicated that equilibrium was reached by 0.5 h for all samples. The dissociation constants were calculated using GraphPad Prism by fitting fluorescence millipolarization ($mP=P\cdot10^{-3}$, where P is polarization) as a function of Sxph concentration using the equation: $P=\{(P_{bound}-P_{free})\ [Sxph]/(K_d+[Sxph])\}+P_{free}$, where P is the polarization measured at a given Sxph concentration, P_{free} is the polarization of Sxph in the absence of F-STX, and P_{bound} is the maximum polarization of Sxph bound by F-STX (*3, 4*).

Isothermal titration calorimetry (ITC)

ITC measurements were performed at 25°C using a MicroCal PEAQ-ITC calorimeter (Malvern Panalytical). *Rc*Sxph, *Rc*Sxph mutants, *Np*Sxph, and *Np*Sxph I559Y were purified using a final size exclusion chromatography step in 150 mM NaCl, 10 mM HEPES, pH 7.4. 1 mM STX stock solution was prepared by dissolving STX powder in MilliQ water. This STX stock was diluted with the SEC buffer to prepare 100 µM or 300 µM STX solutions having a final buffer composition of 135 mM NaCl, 9 mM HEPES, pH 7.4. To match buffers between the Sxph and STX solutions, the purified protein samples were

diluted with MilliQ water to reach a buffer concentration of 135 mM NaCl, 9 mM HEPES, pH 7.4. (30 μM for *Rc*Sxph D794E;10 μM for *Rc*Sxph, other *Rc*Sxph mutants, *Np*Sxph, and *Np*Sxph I559Y) Protein samples were filtered through a 0.22 μm spin filter (Millipore) before loading into the sample cell and titrated with STX (300 μM STX for *Rc*Sxph D794 and 100 μM STX for *Rc*Sxph, other *Rc*Sxph mutants, *Np*Sxph, and *Np*Sxph I559Y) using a schedule of 0.4 μL titrant injection followed by 35 injections of 1 μL for the strong binders (*Rc*Sxph, *Rc*Sxph Y558I, *Rc*Sxph Y558A, *Rc*Sxph F561A, *Np*Sxph, and *Np*Sxph I559Y) and a schedule of 0.4 μL titrant injection followed by 18 injections of 2 μL for the weak binders (*Rc*Sxph P727A, *Rc*Sxph E540D, and *Rc*Sxph D794E). The calorimetric experiment settings were: reference power, 5 μcal/s; spacing between injections, 150 s; stir speed 750 rpm; and feedback mode, high. Data were analyzed using MicroCal PEAQ-ITC Analysis Software (Malvern Panalytical) using a single binding site model. The heat of dilution from titrations of 100 μM STX in 135 mM NaCl, 9 mM HEPES, pH 7.4 into 135 mM NaCl, 9 mM HEPES, pH 7.4 was subtracted from each experiment to correct the baseline.

Crystallization, structure determination, and refinement

*Rc*Sxph mutants were crystallized at 4°C as previously described for *Rc*Sxph (*1*). Briefly, purified protein was exchanged into a buffer of 10 mM NaCl, 10 mM HEPES, pH 7.4 and concentrated to 65 mg ml^{-1} using a 50-kDa cutoff Amicon Ultra centrifugal filter unit (Millipore). Crystallization was set up by hanging drop vapor diffusion using a 24-well VDX plate with sealant (Hampton Research) using 3 μL drops having a 2:1 (v:v) ratio of protein:precipitant. For co-crystallization with STX, STX and the target *Rc*Sxph mutants were mixed in a molar ratio of 1.1:1 STX:Sxph and incubated on ice for 1 hour before setting up crystallization. *Rc*Sxph-Y558I and *Rc*Sxph-Y558I:STX were crystallized from solutions containing 27% (v/v) 2-methyl-2,4-pentanediol, 5% (w/v) PEG 8000, 0.08-0.2 M sodium cacodylate, pH 6.5. *Rc*Sxph-Y558A and *Rc*Sxph-Y558A:STX were crystallized from solutions containing 33% (v/v) 2-methyl-2,4-pentanediol, 5% (w/v) PEG 8000, 0.08-0.2 M sodium cacodylate, pH 6.5. To obtain crystals of the *Rc*Sxph:F-STX complex, *Rc*Sxph was crystallized from solutions containing 33% (v/v) 2methyl-2,4-pentanediol, 5% (w/v) PEG 8000, 0.11-0.2 M sodium cacodylate, pH 6.5 and then soaked with F-STX (final concentration, 1 mM) for 5 hours before freezing.

For *Np*Sxph crystallization, protein was purified as described for *Rc*Sxph, except that the final size exclusion chromatography was done using 30 mM NaCl, 10 mM HEPES, pH

7.4. Protein was concentrated to 30-40 mg ml^{-1} using a 50-kDa cutoff Amicon Ultra centrifugal filter unit (Millipore). *Np*Sxph crystals were obtained by hanging drop vapor diffusion at 4°C using 1:1 v/v ratio of protein and precipitant. *Np*Sxph crystals were obtained from 400 nl drops set with Mosquito crystal (Sptlabtech) using 20-25% (v/v) PEG 400, 4-5% (w/v) PGA-LM, 100-200 mM sodium acetate, pH 5.0. For STX co-crystallization, *Np*Sxph and STX (5 mM stock solution prepared in MilliQ water) were mixed in a molar ratio of 1.2:1 STX:*Np*Sxph and incubated on ice for 1 hour before setting up the crystallization trays. For F-STX soaking, *Np*Sxph crystals were soaked with F-STX (final concentration, 1 mM) for 5 hours before freezing. Crystals of the *Np*Sxph:STX complex were grown in the same crystallization solution as *Np*Sxph. *Np*Sxph, *Np*Sxph:STX, and *Np*Sxph:F-STX crystals were harvested and flash-frozen in liquid nitrogen without additional cryoprotectant.

X-ray datasets for *Rc*Sxph mutants, *Rc*Sxph mutant:STX complexes, *Rc*Sxph: F-STX, *Np*Sxph, and *Np*Sxph:STX were collected at 100K at the Advanced Photon Source (APS) beamline 23 ID B of Argonne National Laboratory (Lemont, IL), processed with XDS (*5*) and scaled and merged with Aimless(*6*). *Rc*Sxph structures were determined by molecular replacement of *Rc*Sxph chain B from (PDB: 6O0F) using Phaser from PHENIX (*7*). The resulting electron density map was thereafter improved by rigid body refinement using phenix.refine. The electron density map obtained from rigid body refinement was manually checked and rebuilt in COOT (*8*) and subsequent refinement was performed using phenix.refine.

The *Np*Sxph structure was solved by molecular replacement using the MoRDa pipeline implemented in the Auto-Rikshaw, automated crystal structure determination platform (*9*). The scaled X-ray data and amino-acid sequence of *Np*Sxph were provided as inputs. The molecular replacement search model was identified using the MoRDa domain database derived from the Protein Data Bank (PDB). The MR solution was refined with REFMAC5 (*10*), density modification was performed using PIRATE(*11, 12*), and was followed by the automated model building in BUCCANEER (*13, 14*). The partial model was further refined using REFMAC5 and phenix.refine. Dual fragment phasing was performed using OASIS-2006 (*12*) based on the automatically refined model, and the resulting phases were further improved in PIRATE. The next round of model building was continued in ARP/wARP (*15*) and the resulting structure was refined in REFMAC5. The final model generated in Auto-Rikshaw (720 out of 825 residues built, and 625 residues automatically docked) was

further used as a MR search model in Phaser from PHENIX (*7*). The quality of the electron density maps allowed an unambiguous assignment of most of the amino acid residues with the exception of the loop regions and the C2 subdomain showing poor electron density. The apo-*Np*Sxph structure was completed by manual model building in COOT (*8*)and multiple rounds of refinement in phenix.refine. The *Np*Sxph:STX: structure was solved by molecular replacement using the *Np*Sxph structure as a search model in Phaser from PHENIX (*7*). After multiple cycles of manual model rebuilding in COOT (*8*), iterative refinement was performed using phenix.refine. The quality of all models was assessed using MolProbity (*16*) and refinement statistics.

RNA sequencing of *O. sylvatica*, *D. tinctorius*, *R. imitator*, *E. tricolor*, *A. femoralis*, and *M. aurantiaca* Sxphs

Nearly all poison frog species were bred in the O'Connell Lab or purchased from the pet trade (Josh's Frogs) except for *O. sylvatica*, which was field collected as described in (*17*). *De novo* transcriptomes for *O. sylvatica*, *D. tinctorius*, *R. imitator*, *E. tricolor*, *A. femoralis*, and *M. aurantiaca* were constructed using different tissue combinations depending on the species. RNA extraction from tissues was performed using TRIzol™ Reagent (Thermo Fisher Scientific). Poly-adenylated RNA was isolated using the NEXTflex PolyA Bead kit (Bioo Scientific, Austin, USA) following manufacturer's instructions. RNA quality and lack of ribosomal RNA was confirmed using an Agilent 2100 Bioanalyzer or Tapestation (Agilent Technologies, Santa Clara, USA). Each RNA sequencing library was prepared using the NEXTflex Rapid RNAseq kit (Bioo Scientific). Libraries were quantified with quantitative PCR (NEBnext Library quantification kit, New England Biolabs, Ipswich, USA) and an Agilent Bioanalyzer High Sensitivity DNA chip, according to manufacturer's instructions. All libraries were pooled at equimolar amounts and were sequenced on four lanes of an Illumina HiSeq 4000 machine to obtain 150 bp paired-end reads. *De novo* transcriptomes were assembled using Trinity and once assembled were used to create a BLAST nucleotide database using the BLAST+ command line utilities. The amino acid Sxph sequence of *R. catesbeiana* was used as a query to tBLASTN against the reference transcriptome databases. The Sxph sequence for *O. sylvatica* was lacking the 5' and 3' ends, whose sequence was obtained using RACE as described above. After obtaining a full-length sequence, the top BLAST hits from each poison frog transcriptome were manually inspected and aligned to the *O. sylvatica* nucleotide sequence to find full sequences with high similarity. Either a single Sxph sequence from each transcriptome

was found to be the best match, or there were multiple transcripts that aligned well, in which case a consensus alignment was created. The largest ORF from each species sequence was translated to create an amino acid sequence for alignment. For the *D. tinctorius*, *R. imitator*, and *A. femoralis* sequences, regions covering the STX binding site and transferrin-related iron-binding sites were confirmed by PCR and sanger sequencing.

Identification of *P. terribilis, R. marina*, *B. bufo*, and *B. gargarizans* Sxphs

All *P. terribilis* frogs were captive bred in the O'Connell lab poison frog colony. All were sexually mature individuals housed in 18x18x18-inch glass terraria, brought up on a diet of *Drosophila melanogaster* without additional toxins. Frogs were euthanized according to the laboratory collection protocol detailed by (*18*) and tissues were stored in RNALater. Eye tissue was rinsed in PBS before being placed into the beadbug tubes (Sigma-Aldrich, Z763756) prefilled with 1 mL TRIzol (Thermo Fisher Scientific, 15596018) and then RNA was extracted following manufacturer instructions. RNA was reverse transcribed into cDNA following the protocol outlined in Invitrogen's SuperScript IV Control Reactions First-Strand cDNA Synthesis reaction (Pub. no. MAN0013442, 16 Rev. B). After reverse transcription, cDNA concentration was checked via NanoDrop (Thermo Scientific, ND-ONE-W), and then aliquoted and stored at -20°C until used for PCR. Saxiphilin was amplified from cDNA from *P. terribilis* in 50 µL polymerase chain reactions following the New England Biolabs protocol for Phusion® High-Fidelity PCR Master Mix with HF Buffer (30) (included DMSO). Each reaction was performed with 1 µL of cDNA. PCR primers were designed based on a *O. sylvatica* saxiphilin cDNA sequence previously generated by the O'Connell lab. PCR products were cleaned up using the Thermo Scientific GeneJET Gel Extraction and DNA Cleanup Micro Kit (Catalog number K0832) dimer removal protocol, and then sent out for Sanger Sequencing via the GeneWiz "Premix" service. The segments from sequencing were aligned and assembled but found that the 5' and 3' ends of the Sxph sequence for *P. terribilis* were missing, thus the 5' and 3' end sequences were subsequently obtained using RACE. 5' and 3'-RACE-Ready cDNA templates were synthesized using a SMARTer® RACE 5'/3' Kit (Takara Bio, USA) and subsequently used to amplify 5' and 3' end sequences of *P. terribilis* Sxph using internal gene specific primers.

Initial Sxph sequence for *R. marina* was obtained from the genome by searching the draft Cane Toad genome (*19*) with tBLASTN using the *R. catesbeiana* Sxph amino acid

sequence as a query. Matching segments from the genome were pieced together to produce an amino acid sequence, however, this sequence was missing part of the 3' end. To obtain the 3' residues, the nucleotide sequences from the genome were used to design primers for 3' Rapid Amplification of cDNA Ends (RACE). One *R. marina* individual from a lab-housed colony was thus euthanized in accordance with UCSF IACUC protocol AN136799, and a portion of the liver was harvested for total RNA extraction using TRIzol™ Reagent (Thermo Fisher Scientific). Total RNA integrity was assessed on a denaturing formaldehyde agarose gel. 3'-RACE-Ready cDNA template was synthesized using a SMARTer® RACE 5'/3' Kit (Takara Bio, USA) and subsequently used to amplify 3' end sequences of *R. marina* Sxph using internal gene specific primers designed from *R. marina* genomic sequences. 3' end sequences of *R. marina* Sxph were determined by gel extraction using QIAquick Gel Extraction Kit (QIAGEN) and verified by sanger sequencing.

Sequences for *Bufo bufo* (CaucascianToad) and *Bufo gargarizans* (Asiatic toad) Sxphs were identified as sequence searches (tBLASTN) using the *Rm*Sph sequence as a query.

Two-electrode voltage clamp electrophysiology

Two-electrode voltage-clamp (TEVC) recordings were performed on defolliculated stage V–VI *Xenopus laevis* oocytes harvested under UCSF-IACUC protocol AN178461. Capped mRNA for *P. terribilis (Pt)* $Na_V1.4$ (GenBank: MZ545381.1) expressed in a pCDNA3.1 vector (*20*) was made using the mMACHINE™ T7 Transcription Kit (Invitrogen). *Xenopus* oocytes were injected with 3–6 ng of *Pt* $Na_V1.4$ and TEVC experiments were performed 1–2 days post-injection. Data were acquired using a GeneClamp 500B amplifier (MDS Analytical Technologies) controlled by pClamp software (Molecular Devices), and digitized at 1 kHz using Digidata 1332A digitizer (MDS Analytical Technologies).

Oocytes were impaled with borosilicate recording microelectrodes (0.3–3.0 MΩ resistance) backfilled with 3 M KCl. Sodium currents were recorded using a bath solution containing the following, in millimolar: 96, NaCl; 1, $CaCl_2$; 1, $MgCl_2$; 2, KCl; and 5, HEPES (pH 7.5 with NaOH), supplemented with antibiotics (50 $\mu g\ ml^{-1}$ gentamycin, 100 IU ml^{-1} penicillin and 100 $\mu g\ ml^{-1}$ streptomycin) and 2.5 mM sodium pyruvate. Sxph responses were measured using Sxph or Sxph mutants purified as described above. Following recording of channel behavior in the absence of toxin, 100 nM STX was applied to achieve ~90% block. Sxph was then added directly to a 1 mL recording chamber containing the toxin to the desired concentration. For all [Sxph]:[STX] ratios, the concentration of the

stock Sxph solution added to the chamber was adjusted so that the volume of the added Sxph solution was less than 1% of the total volume of the recording chamber. All toxin effects were assessed with 60-ms depolarization steps from -120 to 0 mV with a holding potential of -120 mV and a sweep-to-sweep duration of 10 s. Recordings were conducted at room temperature (23 ± 2 °C). Leak currents were subtracted using a P/4 protocol during data acquisition. Data Analysis was performed using Clampfit 10.6 (Axon Instruments) and SigmaPlot (Systat Software).

F-STX synthesis

All reagents were obtained commercially unless otherwise noted. *N,N*-Dimethylformamide (DMF) was passed through two columns of activated alumina prior to use. High-performance liquid chromatography-grade CH_3CN and H_2O were obtained from commercial suppliers. Semi-preparative high-performance liquid chromatography (HPLC) was performed on a Varian ProStar model 210. A high-resolution mass spectrum of F-STX was obtained from the Vincent Coates Foundation Mass Spectrometry Laboratory at Stanford University. The sample was analyzed with HESI-MS by direct injection onto Waters Acquity UPLC and a Thermo Fisher Orbitrap Exploris™ 240 mass spectrometer scanning m/z 100–1000. F-STX was quantified by ^{1}H NMR spectroscopy on a Varian Inova 600 MHz NMR instrument using distilled DMF as an internal standard. A relaxation delay (d1) of 20 s and an acquisition time (at) of 10 s were used for spectral acquisition. The concentration of F-STX was determined by integration of ^{1}H signals corresponding to F-STX and a fixed concentration of the DMF standard.

To an ice-cold solution of saxitoxin-N21-hexylamine (1.4 μmol) in 140 μL of pH 9.5 aqueous bicarbonate buffer (0.2 M aqueous $NaHCO_3$, adjusted to pH 9.5 with 1 M aqueous NaOH) was added a solution of fluorescein NHS-ester, 6-isomer (2.0 mg, 4.2 μmol, 3.0 equiv, Lumiprobe) in 140 μL of DMSO. The reaction flask was stoppered, wrapped in foil, and placed in a sonication bath for 30 s. The reaction mixture was then stirred at room temperature for 4 h. Following this time, the reaction was quenched by the addition of 0.3 mL of 1% aqueous CF_3CO_2H. The reaction mixture was diluted with 1.1 mL of 10 mM aqueous CF_3CO_2H and 0.3 mL of DMSO and filtered through a VWR 0.22 μm PTFE filter. The product was purified by reverse-phase HPLC (Silicycle SiliaChrom dt C18, 5 μm, 10 x 250 mm column, eluting with a gradient flow of 10→40% CH_3CN in 10 mM aqueous CF_3CO_2H over 40 min, 214 nm UV detection). At a flow rate of 4 mL/min, F-STX

had retention time of 31.00 min and was isolated as a dark yellow powder following lyophilization (1.08 μmol, 77%, ^{1}H NMR quantitation).

^{1}H NMR (600 MHz, D_2O) δ 8.05 (d, *J* = 8.1 Hz, 1H), 7.94 (d, *J* = 8.9 Hz, 1H), 7.48 (s, 1H), 6.95 (d, *J* = 9.0 Hz, 2H), 6.79 (s, 2H), 6.67 (dt, *J* = 9.1, 2.2 Hz, 2H), 4.60 (d, *J* = 1.2 Hz, 1H), 4.09–4.05 (m, 1H), 3.89 (dd, *J* = 11.6, 5.2 Hz, 1 H), 3.70 (dt, *J* = 10.1, 5.5 Hz, 1H), 3.64 (dd, *J* = 8.7, 5.4 Hz, 1H), 3.47–3.42 (m, 1H), 3.27 (t, *J* = 6.6 Hz, 2 H), 2.97–2.89 (m, 2H), 2.36–2.33 (m 1H), 2.30–2.24 (m, 1H), 1.48–1.45 (m, 2H), 1.32–1.29 (m, 2H), 1.25–1.21 (m, 4H) ppm. HRMS (ESI$^+$) calcd for $C_{37}H_{41}N_8O_{10}$, 757.2940; found 757.2918 (M^+).

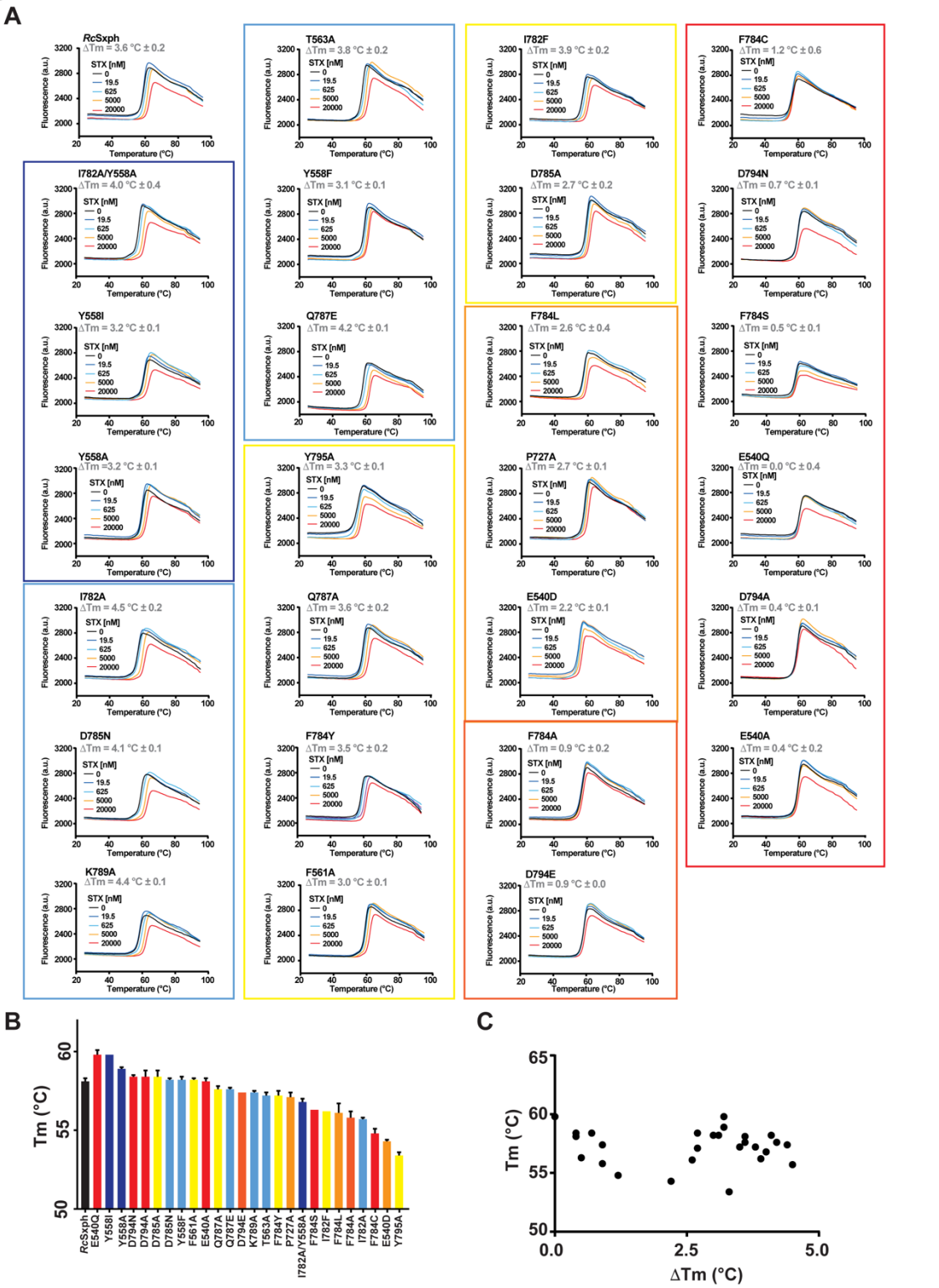

Fig. S1. *Rc*Sxph thermofluor (TF) assay. A, Exemplar thermofluor (TF) assay results for *Rc*Sxph in the presence of the indicated concentrations of STX. Curves for *Rc*Sxph, E540A, P727A, Y558A, F561A, and T563A are identical to those shown in Figs. 1A and 1B. ΔTm values are indicated. **B**, Baseline Tm values for *Rc*Sxph and the indicated mutants. C, Plot of Tm vs. ΔTm for the proteins

in ‘B’. Colored boxes in ‘A’ and bars in ‘B’ correspond to $\Delta\Delta G$ classifications in Table 1. Error bars are S.E.M.

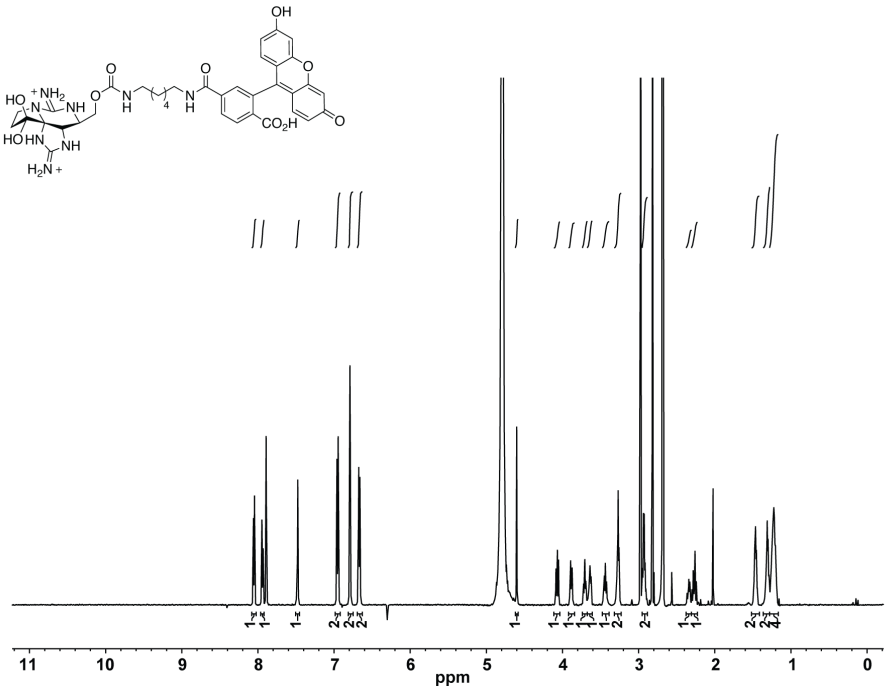

Fig. S2. F-STX NMR spectrum. ^{1}H NMR (600 MHz, D_2O) δ 8.05 (d, *J* = 8.1 Hz, 1H), 7.94 (d, *J* = 8.9 Hz, 1H), 7.48 (s, 1H), 6.95 (d, *J* = 9.0 Hz, 2H), 6.79 (s, 2H), 6.67 (dt, *J* = 9.1, 2.2 Hz, 2H), 4.60 (d, *J* = 1.2 Hz, 1H), 4.09–4.05 (m, 1H), 3.89 (dd, *J* = 11.6, 5.2 Hz, 1 H), 3.70 (dt, *J* = 10.1, 5.5 Hz, 1H), 3.64 (dd, *J* = 8.7, 5.4 Hz, 1H), 3.47–3.42 (m, 1H), 3.27 (t, *J* = 6.6 Hz, 2 H), 2.97–2.89 (m, 2H), 2.36–2.33 (m 1H), 2.30–2.24 (m, 1H), 1.48–1.45 (m, 2H), 1.32–1.29 (m, 2H), 1.25–1.21 (m, 4H) ppm.

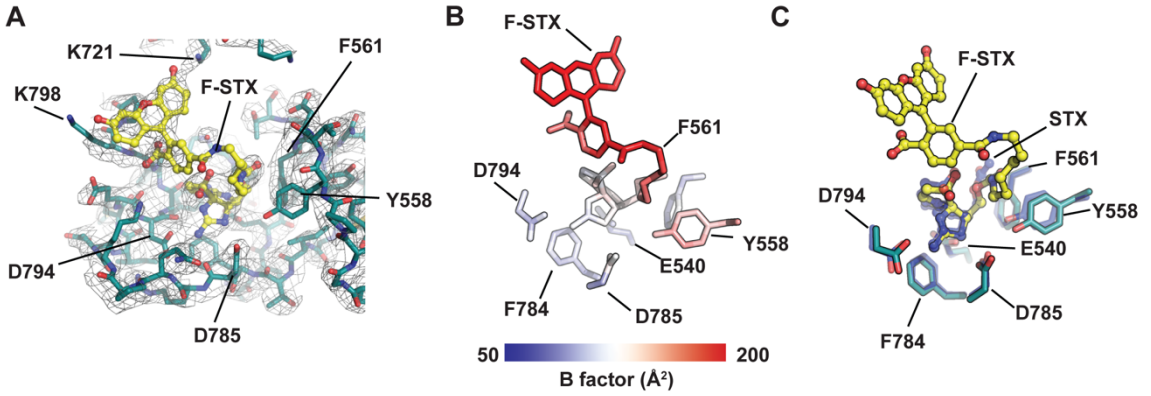

Fig. S3. Structure of the *Rc*Sxph:F-STX complex. A, Exemplar electron density (1σ) for *Rc*Sxph (deep teal) and F-STX (yellow). **B,** *Rc*Sxph:F-STX B-factors for the F-STX ligand and select binding site residues. **C,** Superposition of the STX binding sites of the *Rc*Sxph:F-STX and *Rc*Sxph:STX (PDB:6O0F) (blue) (*1*) complexes.

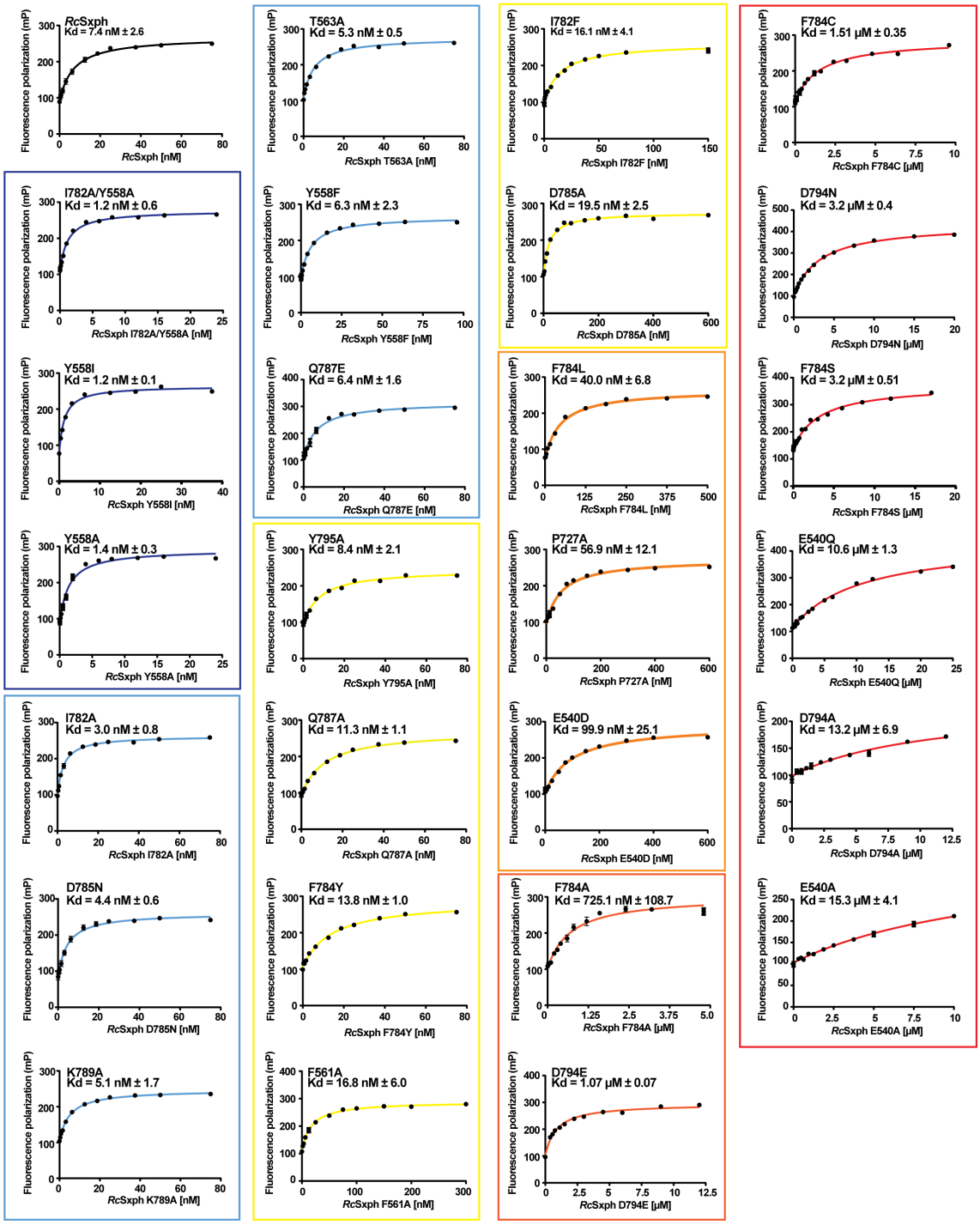

Fig. S4. *Rc*Sxph fluorescence polarization (FP) assay. Exemplar FP binding curves and Kds for *Rc*Sxph and the indicated mutants. Curves for *Rc*Sxph, E540A, P727A, Y558A, F561A, and T563A are identical to those shown in Fig. 1D. Colored boxes and lines in correspond to ΔΔG classifications in Table 1. Error bars are S.E.M.

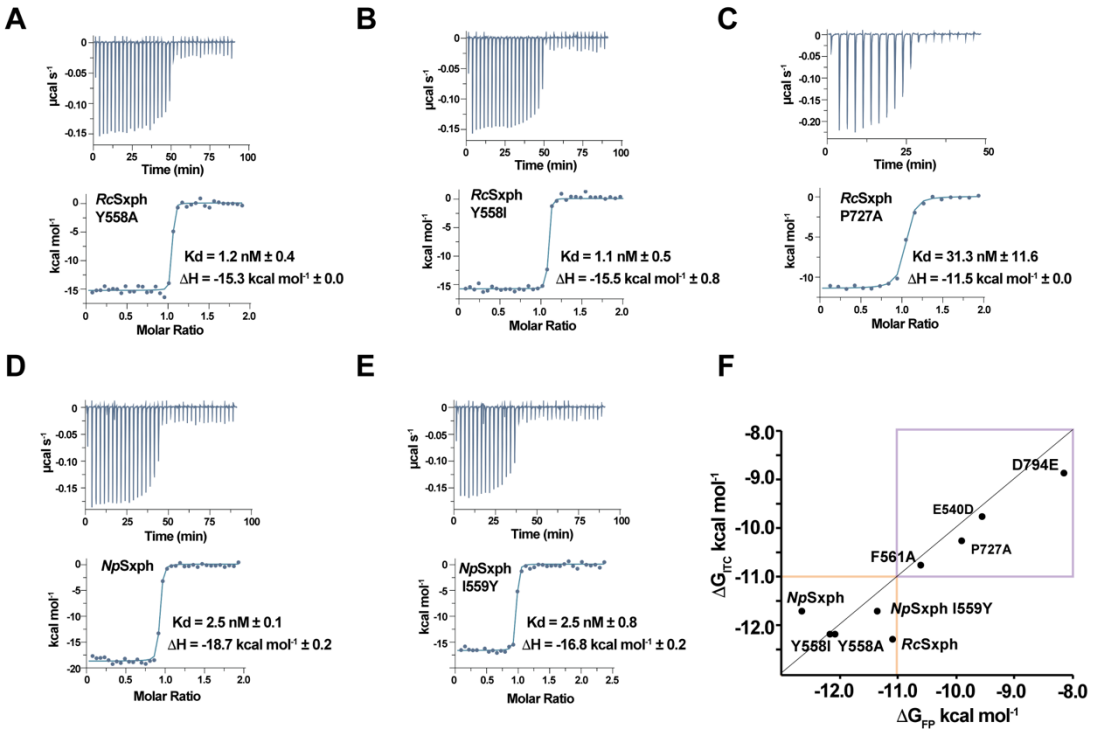

Fig. S5. *Rc*Sxph and *Np*Sxph Isothermal titration calorimetry. Exemplar ITC isotherms for **A,** 100 µM STX into 10 µM *Rc*Sxph Y558A, **B,** 100 µM STX into 10 µM *Rc*Sxph Y558I, C, 100 µM STX into 10 µM *Rc*Sxph P727A, **D,** 100 µM STX into 9.7 µM *Np*Sxph, and E, 100 µM STX into 7.9 µM *Np*Sxph I559Y. **F,** Comparison of ΔG_{ITC} for STX and ΔG_{FP} for F-STX for *Rc*Sxph, *Np*Sxph, and indicated mutants. Purple box highlights region of good correlation. Orange box indicates region outside of the ITC dynamic range. *Rc*Sxph data are identical to Fig. 1G.

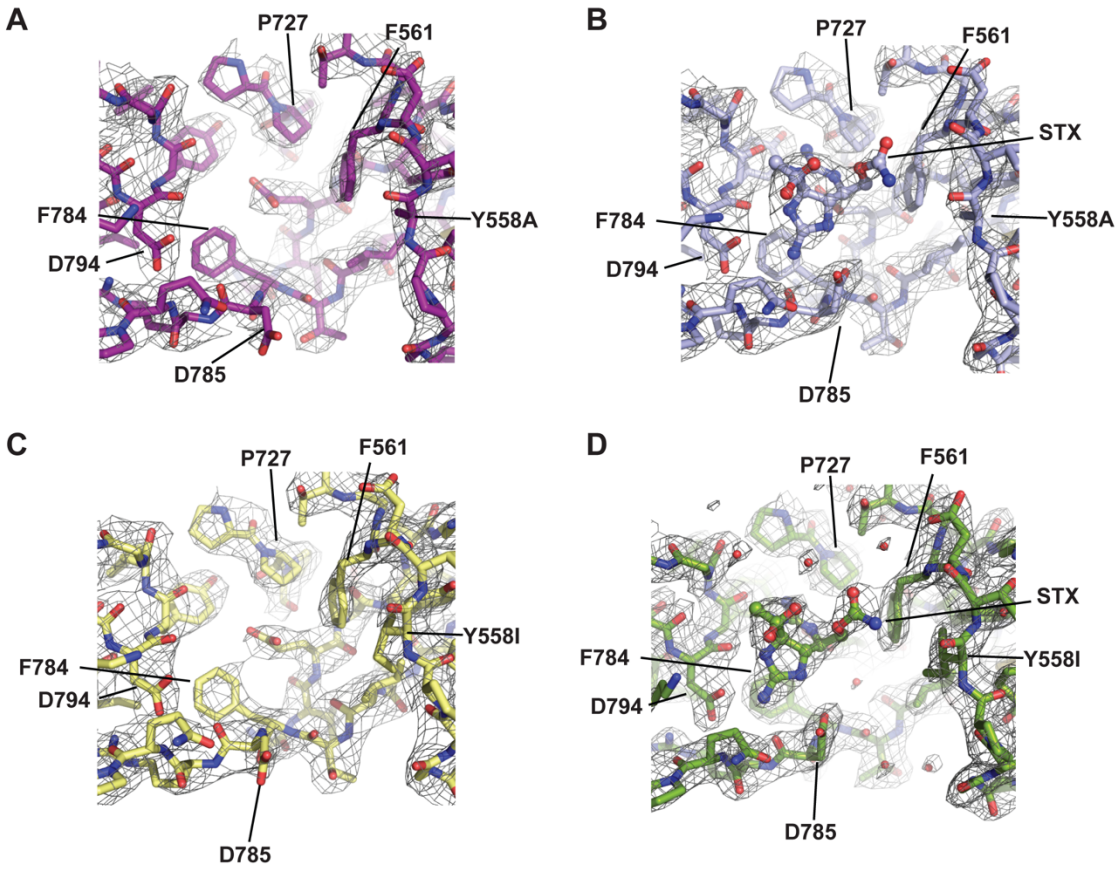

Fig. S6. *Rc*Sxph Y558A and *Rc*Sxph-Y558I structures and STX complexes. Exemplar electron density (1.5 σ) for **A,** *Rc*Sxph Y558A (purple), **B,** *Rc*Sxph-Y558A:STX (light blue), **C,** *Rc*Sxph-Y558I (pale yellow), and **D,** *Rc*Sxph-Y558I:STX (splitpea). Select residues and STX are indicated.

Figure S7 Chen *et al.*

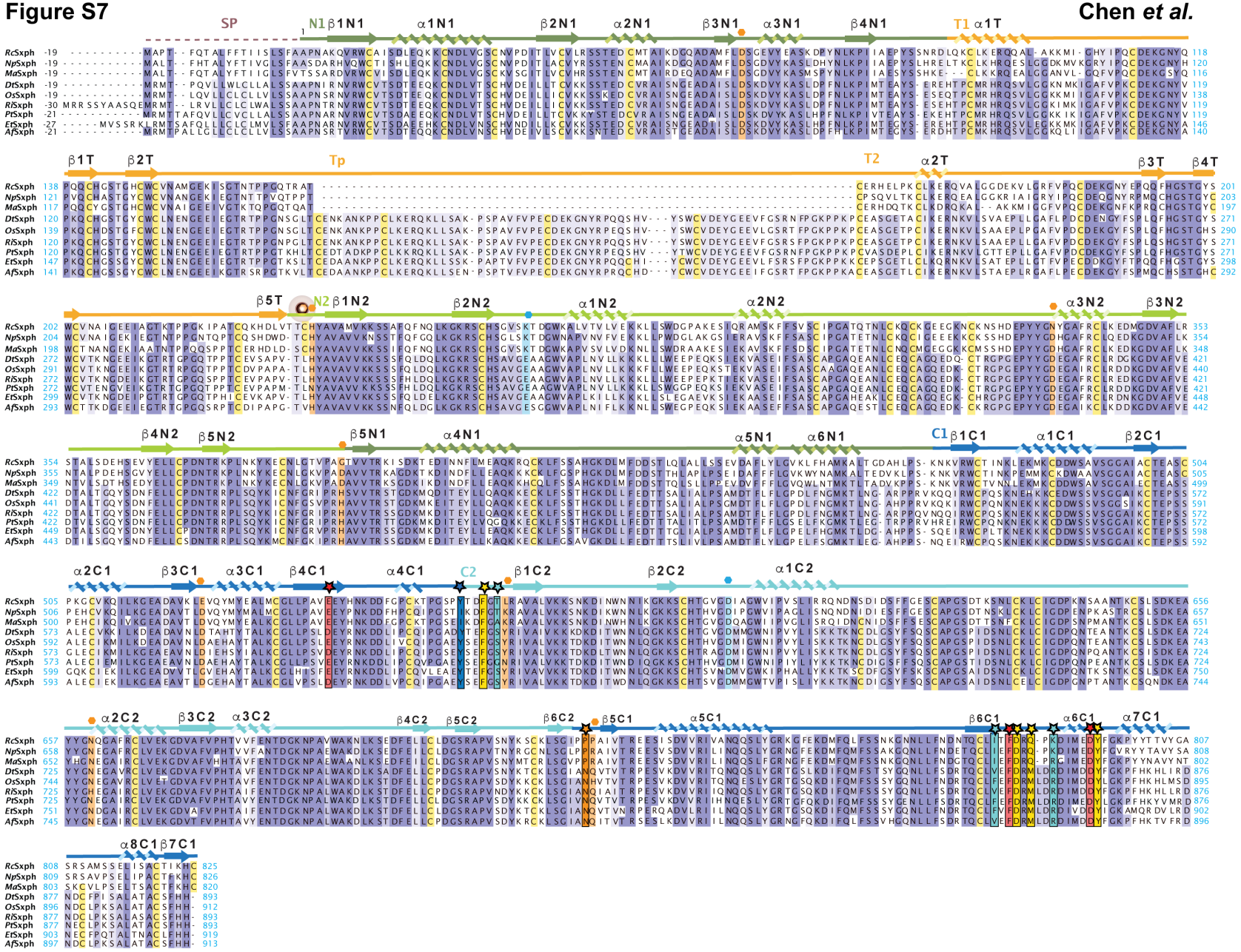

Fig. S7. Frog Sxph sequence alignment. Sxph sequence alignment for *Rc*Sxph, *Np*Sxph, *Ma*Sxph, *Dt*Sxph, *Os*Sxph, *Ri*Sxph, *Pt*Sxph, *Et*Sxph, and *Af*Sxph. Domains and secondary structure are from *Rc*Sxph. N1 (dark green), N2 (light green), Thy1 domains (orange), C1 (marine), C2 (cyan). STX binding site residues are indicated by stars and colored based on the alanine scan results in Table 1. Residues corresponding to transferrin Fe^{3+} and carbonate ligands are indicated by orange and blue hexagons, respectively and highlighted (*1, 21*).

Figure S8 **Chen *et al.***

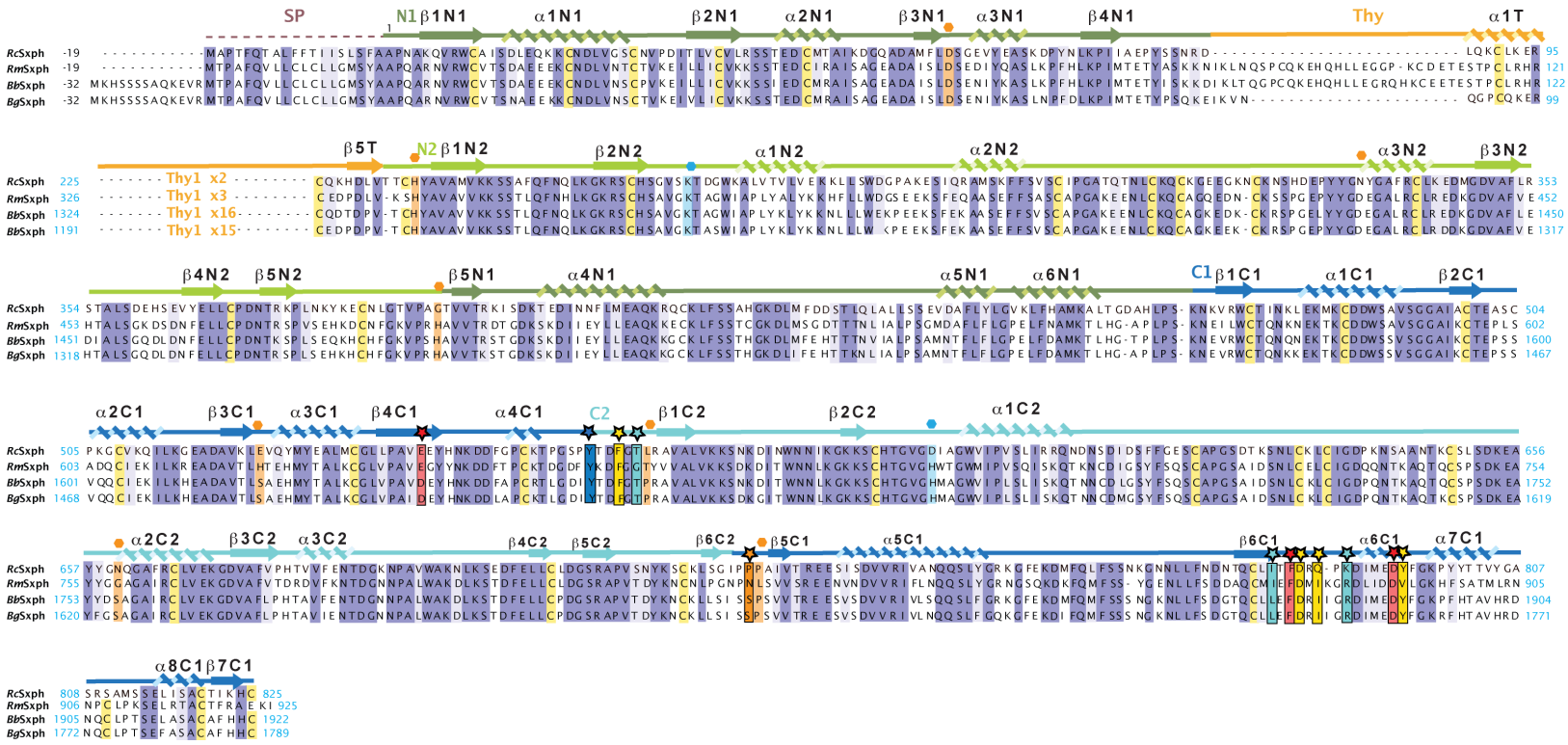

Fig. S8. Toad Sxph sequence alignment. Sxph sequence alignment for *Rc*Sxph, and toad saxiphilins *Rm*Sxph, *Bb*Sxph (NCBI:XM_040427746.1), and *Bg*Sxph(NCBI:XP_044148290.1). Domains and secondary structure are from *Rc*Sxph. N1 (dark green), N2 (light green), Thy1 domains (orange), C1 (marine), C2 (cyan). STX binding site residues are indicated by stars and colored based on the alanine scan results in Table 1. Residues corresponding to transferrin Fe^{3+} and carbonate ligands (*1, 21*) are indicated by orange and blue hexagons, respectively and highlighted. Only beginning and ends of the Thy1 domains are shown. Total number of Thy1 domains are indicated.

Figure S9 **Chen *et al.***

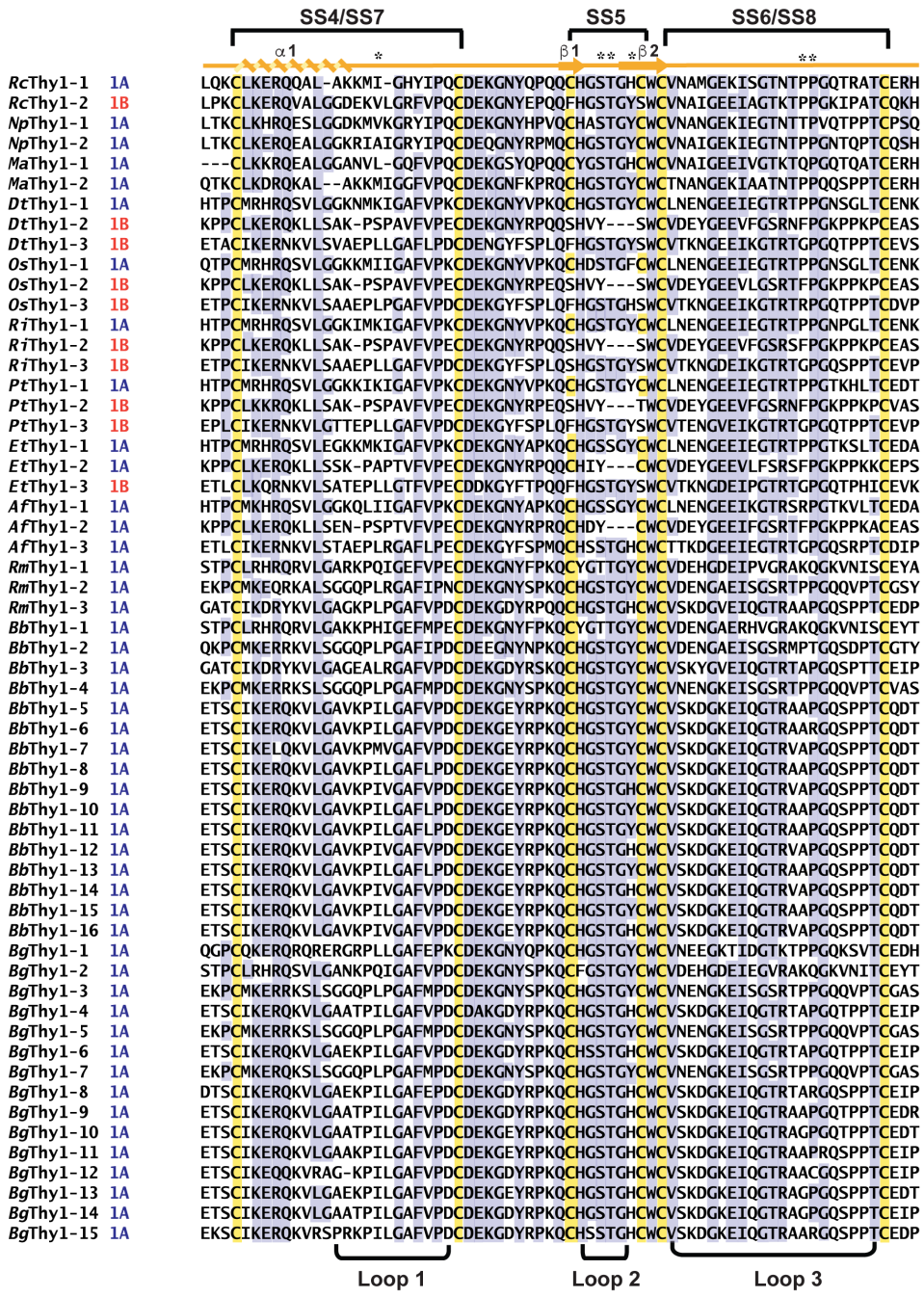

Fig. S9. Thy1 domain sequence alignment. Thy1 domains from *Rc*Sxph, *Np*Sxph, *Ma*Sxph, *Dt*Sxph, *Os*Sxph, *Ri*Sxph, *Pt*Sxph, *Et*Sxph, *Af*Sxph, *Rm*Sxph, *Bb*Sxph, and *Bg*Sxph and the type (1A or 1B) are shown. Secondary structure from *Rc*Sxph Thy1-1 is shown. Cysteine are highlighted. SS4-SS8 indicate disulfide numbers from *Rc*Sxph. Loop regions are indicated.

Figure S10 **Chen *et al.***

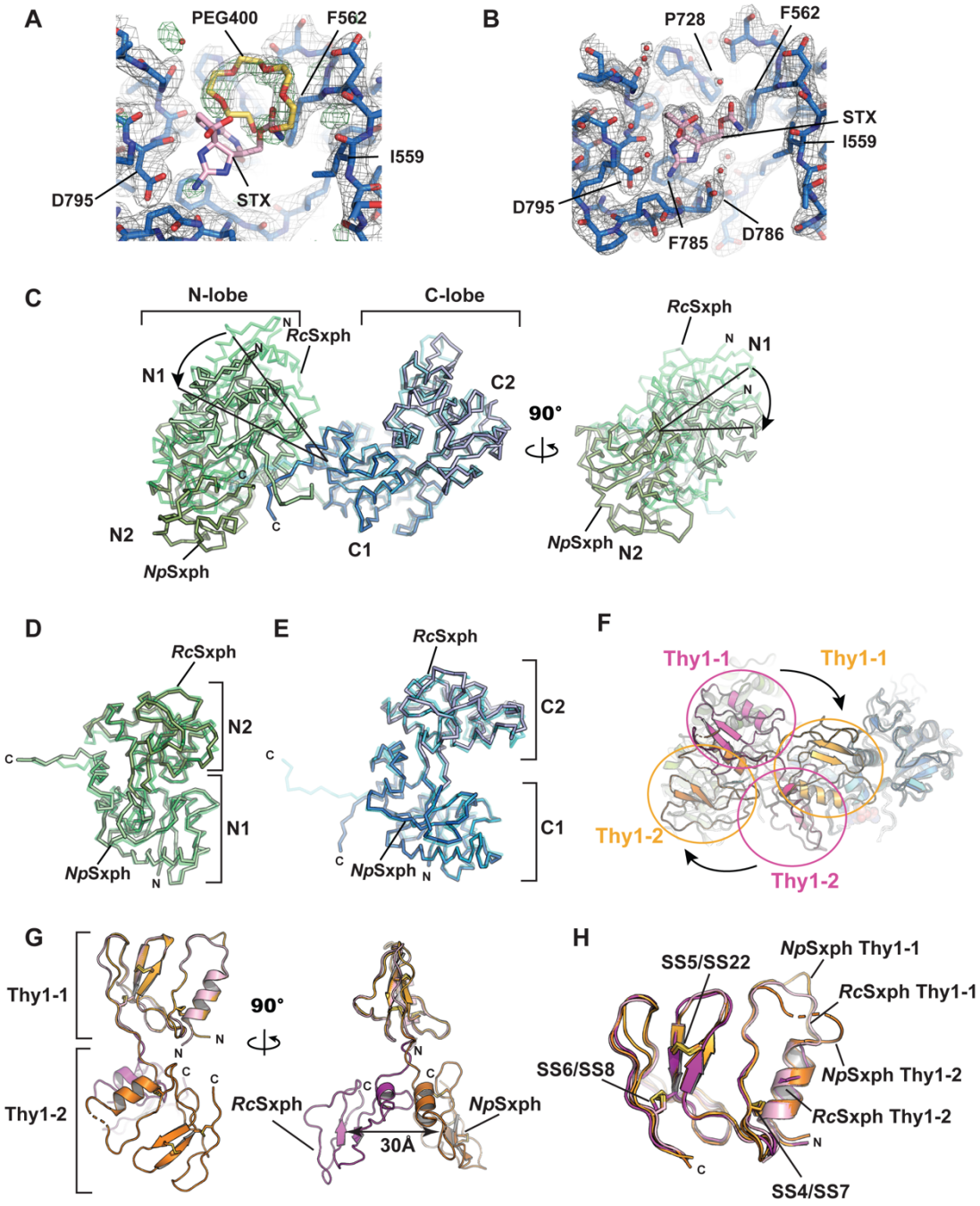

Fig. S10. *Np*Sxph structure and comparisons with *Rc*Sxph. A, and **B,** Exemplar electron density for **A,** *Np*Sxph (2Fo-Fc, 1.5 σ, grey) and (Fo-Fc, 3.0 σ, green). **B,** *Np*Sxph:STX (2Fo-Fc, 1.5 σ, grey). *N*pSxph (marine), STX (pink), and PEG400 (yellow) are shown. STX (pink) from the *Np*Sxph:STX complex is shown in 'A' to compare with the PEG400 position. Select residues are labelled. **C,** *Np*Sxph and *Rc*Sxph superposition using the C-lobes. N- and C-lobes are green/light green and marine/light blue for *Np*Sxph and *Rc*Sxph, respectively. Arrow indicate relationships between *Np*Sxph and *Rc*Sxph N-lobes. **D,** Superposition of *Np*Sxph (green) and *Rc*Sxph (light green) N-lobes. **E,** Superposition of *Np*Sxph (marine) and *Rc*Sxph (light blue) C-lobes. **F,** Cartoon diagram of *Np*Sxph and *Rc*Sxph superposition from 'C' showing the change in Thy1 domain

positions. *N*pSxph Thy1 domains (orange) and *Rc*Sxph Thy1 domains (magenta) are indicated. **G,** Cartoon diagram of *Np*Sxph and *Rc*Sxph Thy1 domains superposed on Thy1-1. *Np*Sxph and *Rc*Sxph Thy1-1 and Thy1-2 are light orange and pink and orange and magenta, respectively. H, Superposition of individual *Np*Sxph and *Rc*Sxph Thy1-1 and Thy1-2 domains. Colors are as in 'G'. Disulfide bonds are indicated. Comparisons are made using the STX bound structures *Np*Sxph (PDB: 8D6M) and *Rc*Sxph (PDB: 6O0F) (*1*).

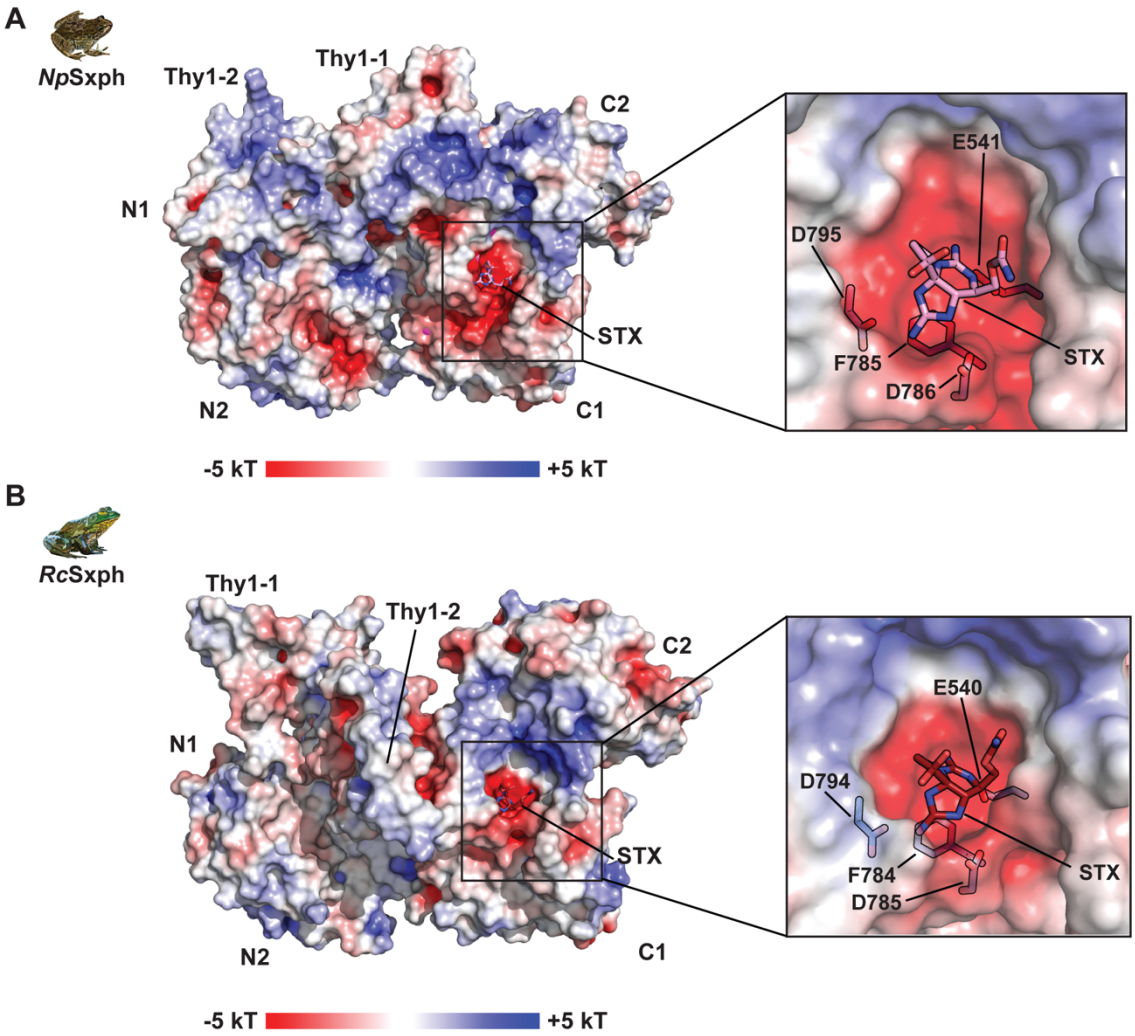

Fig. S11. Electrostatic surface potentials for A, *Np*Sxph (PDB: 8D6M) and **B,** *Rc*Sxph (PDB: 6O0F) (*1*) calculated using APBS (*22*) for the STX bound conformations in the absence of STX. Insets show STX binding pocket with select residues indicated. STX is shown as sticks (**A**, pink, and **B**, firebrick).

Figure S12 **Chen *et al.***

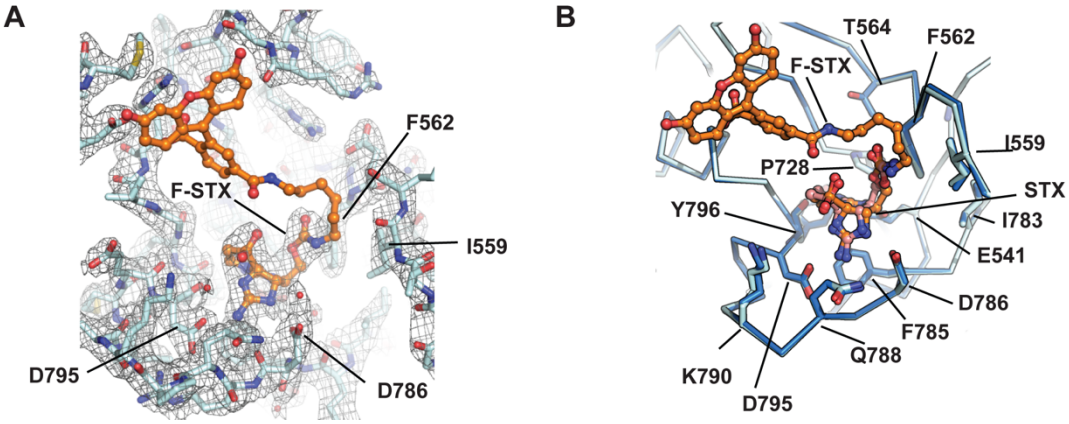

Fig. S12. Structure of the *Np*Sxph:F-STX complex. A, Exemplar electron density for *Np*Sxph:F-STX (2Fo-Fc, 1.5 σ, grey). *Np*Sxph (cyan) and F-STX (orange). **B,** Comparison of *Np*Sxph:STX (marine) and *Np*Sxph:F-STX STX binding sites. STX from *Np*Sxph is pink. F-STX is orange. Select residues are indicated.

Table S1 Crystallographic data collection and refinement statistics				
	***Rc*Sxph -Y558A PDB:8D6P**	***Rc*Sxph -Y558A:STX (co-crystal) PDB:8D6S**	***Rc*Sxph -Y558I PDB:8D6Q**	***Rc*Sxph -Y558I:STX (co-crystal) PDB:8D6T**
Data Collection				
Space group	$P2_12_12_1$	$P2_12_12_1$	$P2_12_12_1$	$P2_12_12_1$
Cell dimensions a/b/c (Å)	96.61, 109.05, 254.89	95.98, 107.14, 253.04	96.39, 107.15, 254.79	96.03, 107.81, 253.58
α/β/γ (°)	90, 90, 90	90, 90, 90	90, 90, 90	90, 90, 90
Resolution (Å)	47.81-2.60 (2.65-2.60)	47.37-2.60 (2.65-2.60)	47.61-2.70 (2.76-2.70)	47.5-2.15 (2.19-2.15)
Rmerge (%)	0.108 (4.094)	0.115 (3.964)	0.159 (4.833)	0.089 (1.558)
I / σ I	12.9 (0.9)	12.5 (0.8)	8.8 (0.6)	16.2 (1.2)
CC(1/2)	0.998 (0.532)	0.998 (0.458)	0.998 (0.419)	0.999 (0.599)
Completeness (%)	99.6 (100)	99.9 (100)	99.9 (99.8)	99.5 (93.6)
Redundancy	13.4 (13.9)	13.4 (14.0)	13.3 (14.0)	12.2 (6.2)
Total reflections	1116931 (62978)	1085831 (61318)	975607 (62994)	1736282 (40652)
Unique reflections	83173 (4517)	81054 (4377)	73319 (4504)	142848 (6596)
Wilson B-factor	83.42	84.83	90.34	44.01
Wavelength (Å)	1.033	1.033	1.033	1.033
Refinement				
R_{work} / R_{free} (%)	22.79/26.37	23.20/26.17	23.42/27.21	20.73/23.37
No. of chains in AU	2	2	2	2
No. of protein atoms	12616	12616	12622	12622
No. of ligand atoms	0	42	0	72
No. of water atoms	77	60	79	794
RMSD bond lengths (Å)	0.002	0.002	0.003	0.003
RMSD angles (°)	0.50	0.49	0.55	0.59
Ramachandran favored/allowed/outliers (%)	94.90/4.91/0.18	94.29/5.47/0.25	93.61/6.08/0.31	95.33/4.30/0.37

Table S1 Crystallographic data collection and refinement statistics (continued)				
	***Rc*Sxph:F-STX (soaked) PDB:8D6U**	***Np*Sxph PDB:8D6G**	***Np*Sxph:STX (co-crystal) PDB:8D6M**	***Np*Sxph:F-STX (soaked) PDB:8D6O**
Data Collection				
Space group	$P2_12_12_1$	R3	R3	R3
Cell dimensions a/b/c (Å)	96.44, 109.37, 256.36	229.046, 229.046, 67.428	228.848, 228.848, 67.224	229.186, 229.186, 67.347
α/β/γ (°)	90, 90, 90	90, 90, 120	90, 90, 120	90, 90, 120
Resolution (Å)	47.97-2.65 (2.70-2.65)	43.29-2.2 (2.279-2.2)	42.55-2.0 (2.071-2.0)	43.31-2.2 (2.279-2.2)
Rmerge (%)	0.112 (4.136)	0.05218 (0.8687)	0.05456 (0.9961)	0.07078 (1.889)
I / σ I	11.1 (0.8)	12.66 (0.89)	14.11 (1.11)	19.64 (1.35)
CC(1/2)	0.999 (0.513)	0.999 (0.465)	0.998 (0.637)	0.999 (0.602)
Completeness (%)	99.9 (99.8)	98.60 (91.37)	99.89 (99.61)	99.90 (99.97)
Redundancy	10.4 (11.0)	3.3 (2.1)	5.2 (4.8)	10.6 (11.0)
Total reflections	830262 (49019)	219806 (12669)	459480 (42277)	707304 (73200)
Unique reflections	79524 (4469)	66067 (6127)	88641 (8856)	66898 (6682)
Wilson B-factor	83.73	52.73	49.89	55.11
Wavelength (Å)	1.033	1.033167	1.033167	1.033167
Refinement				
R_{work} / R_{free} (%)	23.46/26.51	19.50/23.55	19.25/22.09	19.64/24.26
No. of chains in AU	2	1	1	1
No. of protein atoms	12630	6373	6385	6346
No. of ligand atoms	110	38	59	93
No. of water atoms	88	229	287	161
RMSD bond lengths (Å)	0.002	0.004	0.004	0.006
RMSD angles (°)	0.50	0.60	0.62	0.75
Ramachandran favored/allowed/outliers (%)	94.23/5.41/0.37	95.71/4.17/0.12	95.85/3.90/0.24	94.19/5.56/0.25

Table S2 *Rc*Sxph:STX and *Np*Sxph:STX thermodynamic binding parameters

		N (sites)	Kd (nM)	ΔH (kcal mol^{-1})	ΔS (cal mol^{-1} K^{-1})	ΔG (kcal mol^{-1})	n
*Rc*Sxph	***WT***	1.02 ± 0.01	1.2 ± 0.8	-16.1 ± 0.2	-12.7 ± 0.9	-12.3 ± 0.5	3
	Y558A	1.01 ± 0.01	1.2 ± 0.4	-15.3 ± 0.0	-11.1 ± 1.1	-12.2 ± 0.2	2
	Y558I	1.05 ± 0.03	1.1 ± 0.5	-15.5 ± 0.3	-10.5 ± 0.6	-12.2 ± 0.3	2
	F561A	1.07 ± 0.01	13.4 ± 1.4	-12.7 ± 0.2	-6.6 ± 0.9	-10.8 ± 0.1	3
	P727A	0.97 ± 0.03	31.3 ± 11.6	-11.5 ± 0.0	-4.2 ± 0.9	-10.3 ± 0.2	2
	E540D	0.98 ± 0.02	68.9 ± 10.7	-16.3 ± 1.7	-21.9 ± 5.7	-9.8 ± 0.1	4
	D794E	0.99 ± 0.01	312.5 ± 2.9	-11.8 ± 0.0	-8.9 ± 0.1	-8.9 ± 0.1	2
*Np*Sxph	***WT***	0.92 ± 0.02	2.5 ± 0.1	-18.7 ± 0.2	-23.2 ± 0.8	-11.8 ± 0.1	2
	I559Y	0.94 ± 0.03	2.5 ± 0.8	-16.8 ± 0.2	-16.9 ± 1.1	-11.8 ± 0.2	4

Movie S1 (separate file). *Rc*Sxph-Y558A conformational changes upon STX binding. Morph between the apo-*Rc*Sxph-Y558A and *Rc*Sxph-Y558A:STX structures showing the STX binding pocket. Sidechains are shown as sticks. STX is red.

Movie S2 (separate file). *Rc*Sxph-Y558I conformational changes upon STX binding. Morph between the apo-*Rc*Sxph-Y558I and *Rc*Sxph-Y558A:STX structures showing the STX binding pocket. Sidechains are shown as sticks. STX is red.

Movie S3 (separate file). Conformational changes between *Rc*Sxph and *Np*Sxph. Morph between apo-*Rc*Sxph (PDB:6O0D) (*1*) (starting structure) and apo-*Np*Sxph (final structure). N-lobe (green), C-lobe (blue), and Thy domains (magenta) are shown. N1, N2, C1, and C2 subdomains and Thy1-1, and Thy1-2 are labeled.

Movie S4 (separate file). *Np*Sxph conformational changes upon STX binding. Morph between the apo-*Np*Sxph and *Np*Sxph:STX structures showing the STX binding pocket. Sidechains are shown as sticks. STX is red.

SI References

1. T.-J. Yen, M. Lolicato, R. Thomas-Tran, J. Du Bois, D. L. Minor, Jr., Structure of the Saxiphilin:saxitoxin (STX) complex reveals a convergent molecular recognition strategy for paralytic toxins. *Sci Adv* **5**, (2019).
2. K. Huynh, C. L. Partch, Analysis of protein stability and ligand interactions by thermal shift assay. *Curr Protoc Protein Sci* **79**, 28 29 21-14 (2015).
3. A. M. Rossi, C. W. Taylor, Analysis of protein-ligand interactions by fluorescence polarization. *Nat Protoc* **6**, 365-387 (2011).
4. S. Hansen *et al.*, Regulation of the Escherichia coli HipBA toxin-antitoxin system by proteolysis. *PLoS One* **7**, e39185 (2012).
5. W. Kabsch, Xds. *Acta Crystallogr D Biol Crystallogr* **66**, 125-132 (2010).
6. P. R. Evans, G. N. Murshudov, How good are my data and what is the resolution? *Acta Crystallogr D Biol Crystallogr* **69**, 1204-1214 (2013).
7. P. D. Adams *et al.*, PHENIX: a comprehensive Python-based system for macromolecular structure solution. *Acta Crystallogr D Biol Crystallogr* **66**, 213-221 (2010).
8. P. Emsley, K. Cowtan, Coot: model-building tools for molecular graphics. *Acta Crystallogr D Biol Crystallogr* **60**, 2126-2132 (2004).
9. S. Panjikar, V. Parthasarathy, V. S. Lamzin, M. S. Weiss, P. A. Tucker, Auto-rickshaw: an automated crystal structure determination platform as an efficient tool for the validation of an X-ray diffraction experiment. *Acta Crystallogr D Biol Crystallogr* **61**, 449-457 (2005).
10. N. Collaborative Computational Project, The CCP4 suite: Programs for protein crystallography. *Acta Crystallogr D Biol Crystallogr* **50**, 760-763. (1994).
11. K. Cowtan, General quadratic functions in real and reciprocal space and their application to likelihood phasing. *Acta Crystallogr D Biol Crystallogr* **56**, 1612-1621 (2000).
12. M. D. Winn *et al.*, Overview of the CCP4 suite and current developments. *Acta Crystallogr D Biol Crystallogr* **67**, 235-242 (2011).
13. K. Cowtan, The Buccaneer software for automated model building. 1. Tracing protein chains. *Acta Crystallogr D Biol Crystallogr* **62**, 1002-1011 (2006).
14. K. Cowtan, Fitting molecular fragments into electron density. *Acta Crystallogr D Biol Crystallogr* **64**, 83-89 (2008).
15. R. J. Morris *et al.*, Breaking good resolutions with ARP/wARP. *J Synchrotron Radiat* **11**, 56-59 (2004).
16. C. J. Williams *et al.*, MolProbity: More and better reference data for improved all-atom structure validation. *Protein Sci* **27**, 293-315 (2018).
17. J. R. McGugan *et al.*, Ant and Mite Diversity Drives Toxin Variation in the Little Devil Poison Frog. *J Chem Ecol* **42**, 537-551 (2016).
18. E. K. Fischer *et al.*, Mechanisms of Convergent Egg Provisioning in Poison Frogs. *Curr Biol* **29**, 4145-4151 e4143 (2019).
19. R. J. Edwards *et al.*, Draft genome assembly of the invasive cane toad, Rhinella marina. *Gigascience* **7**, (2018).
20. F. Abderemane-Ali *et al.*, Evidence that toxin resistance in poison birds and frogs is not rooted in sodium channel mutations and may rely on "toxin sponge" proteins. *J Gen Physiol* **153**, (2021).

21. L. A. Lambert, H. Perri, P. J. Halbrooks, A. B. Mason, Evolution of the transferrin family: conservation of residues associated with iron and anion binding. *Comp Biochem Physiol B Biochem Mol Biol* **142**, 129-141 (2005).

22. N. A. Baker, D. Sept, S. Joseph, M. J. Holst, J. A. McCammon, Electrostatics of nanosystems: application to microtubules and the ribosome. *Proc Natl Acad Sci U S A* **98**, 10037-10041 (2001).